



Structural, Electrochemical and Hydrogen Sorption Studies of Nanocrystalline Ti-V-Co and Ti-V-Ni-Co Alloys Synthesized by Mechanical Alloying Method

M. Balcerzak 

(Submitted February 4, 2019; in revised form June 26, 2019; published online August 12, 2019)

In this paper, Ti-V-Co and Ti-V-Ni-Co alloys are considered as the hydrogen storage systems and the negative electrodes in Ni-MH_x secondary batteries. This work shows results of studies that have been made on Ti_{0.5}V_{1.5-x}Co_x and Ti_{0.5}V_{1.4-x}Ni_{0.1}Co_x nanocrystalline alloys ($x = 0, 0.1, 0.2, 0.3$) synthesized by the mechanical alloying technique. The goal of this study is to determine an effect of partial replacement of V by Co atoms on hydrogen storage and electrochemical properties of Ti-V and Ti-V-Ni alloys. X-ray diffraction studies have proven that 14 h of the ball milling has resulted in crystallization of body-centered-cubic solid solution. Studies performed on high-resolution transmission electron microscope confirm creation of nanocrystalline materials. Hydrogen sorption/desorption measurements that have been performed at 303 K show that Co accelerates the hydrogen sorption process, diminishes hysteresis and ameliorates the hydrogen storage reversibility. Properties of Ti-V-Co alloys, described in this work, originate mainly from structure of these materials. Electrochemical measurements of Ti-V-Co alloys have shown these materials poorly absorb hydrogen in 6 M KOH solution. Ti_{0.5}V_{1.4-x}Ni_{0.1}Co_x alloys are characterized by better activation properties and improved cyclability in comparison to Co-free Ti_{0.5}V_{1.4}Ni_{0.1} alloy.

Keywords ball milling, electrode materials, energy, hydrogen storage alloy, nanomaterials, Ni-MH secondary batteries, V-based solid solution alloys

1. Introduction

Body-centered-cubic (BCC) solid solutions have been studied for more than twenty years according to their possible usage as the hydrogen storage system and the secondary battery materials. Ti-V BCC alloys have usually been obtained by the traditional techniques—arc or induction melting. As a result of implementation of these methods, alloys that are characterized by microcrystalline structure are synthesized (Ref 1-3). However, different melting temperatures of constituting elements make the planned chemical composition hard (or sometimes even impossible) to achieve using arc or induction melting. Furthermore, the application of these alloys is restricted by difficult activation and slow hydrogen sorption and desorption process (Ref 1).

I have recently synthesized V-rich BCC solid solutions through the mechanical alloying (MA) (Ref 4). The effect of use of MA method was the creation of the nanocrystalline BCC alloy which absorbed 3.67 wt.% of hydrogen at near room temperature. However, electrochemical studies that were made

on these alloys have shown that they do not perform any electrochemical discharge ability as negative electrodes in Ni-MH_x secondary batteries. It resulted from the fact that V-rich BCC solid solution hydride phase was too stable to desorb hydrogen in moderate conditions. Moreover, the usage of V-rich alloys is limited due to the fact that vanadium is an expensive element (Ref 4).

One of the approaches to overcome these drawbacks is partial substitution of Ti and/or V by other elements (Ref 5-7). One of these elements is Co which improves durability and cyclability of materials by inhibiting the oxidation of electrode (made of BCC alloys) in KOH solution and by improving the anti-pulverization ability (Ref 6, 8, 9). The other one is Ni which was used to reduce the stability of BCC solid solution hydride phase. The recently published paper has shown that even small addition of Ni can make the BCC alloy a material working as the electrode in Ni-MH_x secondary batteries (Ref 10).

However, publications published so far consider the effect of modification by Co atoms on properties of Laves phases-related BCC solid solution (Ref 9, 11, 12). In the literature, there is no paper that considers the influence of Co modification on single-phase BCC solid solution. There are also no publications on Ti-V-Co or Ti-V-Ni-Co BCC solid solutions prepared straight from MA. Therefore, this paper presents results of structural, electrochemical and hydrogen sorption studies of MA Ti_{0.5}V_{1.5-x}Co_x ($x = 0, 0.1, 0.2, 0.3$) and Ti_{0.5}V_{1.4-x}Ni_{0.1}Co_x ($x = 0, 0.1, 0.2, 0.3$) alloys.

2. Experimental Procedure

Mercantile materials were used for synthesis: titanium powder (Alfa Aesar, – 325 mesh, 99.5%), vanadium powder (Alfa Aesar, – 325 mesh, 99.5%), cobalt powder (Alfa Aesar,

Electronic supplementary material The online version of this article (<https://doi.org/10.1007/s11665-019-04266-x>) contains supplementary material, which is available to authorized users.

M. Balcerzak, Institute of Materials Science and Engineering, Poznan University of Technology, Jana Pawła II No 24, 61-138 Poznan, Poland. Contact e-mail: mateusz.balcerzak@put.poznan.pl.

1.6 μm , 99.8%), nickel powder (Aldrich, 5 μm , 99.99%). 6 mol KOH solution was an electrolyte in electrochemical studies.

MA process was used to prepare $\text{Ti}_{0.5}\text{V}_{1.5-x}\text{Co}_x$ alloys ($x = 0, 0.1, 0.2, 0.3$). Binary Ti-V alloy was chosen according to data published in the previous publication— $\text{Ti}_{0.5}\text{V}_{1.5}$ was the alloy with the lowest thermal stability of its hydride phase. MA finished after 14 h of milling in pure argon. The ball-to-powder weight ratio was around 6.5:1. Stainless steel balls were used. MA was stopped every 1 h to dissipate a heat and to reduce an excessive rise in temperature. All details about the MA are included in the already published paper (Ref 4).

Due to the very poor electrochemical properties of Ti-V-Co alloys (which are described below), a group of $\text{Ti}_{0.5}\text{V}_{1.4-x}\text{Ni}_{0.1}\text{Co}_x$ alloys was synthesized. A part of V was substituted by Ni because of good catalytic properties of Ni element (Ref 9). The synthesis of alloys containing Ni was performed in the same way as in the case of Ti-V-Co alloys.

The structure of synthesized $\text{Ti}_{0.5}\text{V}_{1.5-x}\text{Co}_x$ and $\text{Ti}_{0.5}\text{V}_{1.4-x}\text{Ni}_{0.1}\text{Co}_x$ powders was characterized to find the relation with the results of hydrogen sorption and electrochemical measurements. The structure of MA V-rich alloy powders was studied by Panalytical Empyrean diffractometer (Cu $K\alpha_1$ radiation, $\lambda = 1.5405952 \text{ \AA}$, 45 kV, 40 mA). X-ray diffraction (XRD) studies were carried out at room temperature. Moreover, XRD was used to study Ti-V-Co alloys saturated with hydrogen. X-ray diffractograms were analyzed by the Rietveld refinement Maud software. XRD data and Williamson-Hall style plot were used to estimate the average crystallite size and the lattice strain.

The microstructures were examined by scanning electron microscopy (SEM), and analysis of chemical compositions was performed using energy dispersive x-ray spectrometer (EDS)—Tescan VEGA TS5135. Obtained SEM micrographs were used to make particle size dimension distribution histograms. Transmission electron microscope—TEM (Philips CM 20 Super Twin TEM microscope) and high-resolution TEM—HRTEM (Joel ARM 200F microscope) was used to perform the microstructure analysis of unmodified MA $\text{Ti}_{0.5}\text{V}_{1.5}$ alloy.

HPVA-200, Particulate Systems was used to study the hydrogenation and dehydrogenation performances of $\text{Ti}_{0.5}\text{V}_{1.5-x}\text{Co}_x$ powders. The full description of used device is presented in the previously published paper (Ref 4). Hydrogenation and dehydrogenation studies were not preceded by any activation procedure. The only treatment before the measurements was degassing at 303 K for 1 h under vacuum. In the next step, kinetic studies (3 MPa hydrogen pressure, 303 K) were done. After completing the kinetic studies, degassed alloys were measured at 303 K to get pressure-composition isotherm curves of Ti-V and Ti-V-Co alloys.

$\text{Ti}_{0.5}\text{V}_{1.5-x}\text{Co}_x$ alloys in hydrogenated state were studied by differential scanning calorimetry (DSC)—TA DSC Q20. Every sample that was measured by DSC is the one that was previously studied for hydrogen storage properties. Ti-V-Co solid solutions were heated in argon up to 873 K with heating rate of 10 K min^{-1} .

All synthesized Ti-V-Co and Ti-V-Ni-Co samples were mixed with carbonyl nickel powder (10 wt.%) to create a material for negative electrodes in Ni-MH_x secondary batteries. Electrodes were charged and discharged at 40 mA/g. A cut-off potential versus Hg/HgO/6MKOH was -0.7 V . The full description of electrochemical measurements can be found in

previously published paper (Ref 13). The cyclability after 50th cycle was estimated by R_h rate defined as

$$R_h = (C_{50}C_{\max}^{-1}) \times 100\%,$$

where C_{50} and C_{\max} are capacities at the 50th cycle and the largest capacity, respectively.

3. Results and Discussion

3.1 Phase Structures and Microstructures

Figure 1 presents x-ray diffraction patterns of $\text{Ti}_{0.5}\text{V}_{1.5-x}\text{Co}_x$ alloys powders ($x = 0, 0.1, 0.2, 0.3$) after 14 h of MA. All alloys are single-phase BCC solid solution materials which crystallize in a $\text{Im-}3\text{m}$ space group. A single-phase BCC structure was not previously obtained for arc or inductive melted Ti-V-Co and Ti-V-Ni-Co alloys. For these materials, a minor Ti_2Ni and TiCo phases have always been observed (Ref 5, 6).

The intensity of solid solution peaks decreases while the Co content in the material became larger. Peaks also shifted to higher angles positions with the increase of Co content in $\text{Ti}_{0.5}\text{V}_{1.5-x}\text{Co}_x$ alloys. It is due to the decrease of BCC phase cell volume that results from different values of cobalt and vanadium radius (Co—0.125 nm; V—0.134 nm). While increasing the x in $\text{Ti}_{0.5}\text{V}_{1.5-x}\text{Co}_x$, the more smaller Co atoms substitute larger V atoms, and therefore, the cell unit shrinks. The change of lattice parameter in a function of Co content in $\text{Ti}_{0.5}\text{V}_{1.5-x}\text{Co}_x$ alloys is presented in Fig. 2, and the refined lattice parameters are listed in Table 1. The lattice parameter according to the Vegard's law changes linearly with increasing Co content in the alloy.

Chemical modification affected the average crystallite size of $\text{Ti}_{0.5}\text{V}_{1.5-x}\text{Co}_x$ alloys. The size equalled 5.4, 9.2, 10.8, 33.4 nm for $\text{Ti}_{0.5}\text{V}_{1.5}$, $\text{Ti}_{0.5}\text{V}_{1.4}\text{Co}_{0.1}$, $\text{Ti}_{0.5}\text{V}_{1.3}\text{Co}_{0.2}$ and $\text{Ti}_{0.5}\text{V}_{1.2}\text{Co}_{0.3}$ alloy, respectively. A similar tendency was

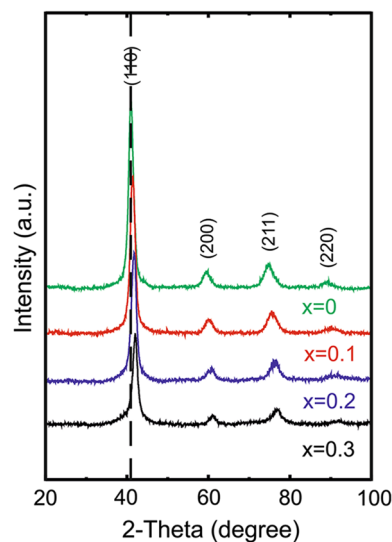


Fig. 1 X-ray diffractograms obtained for mechanically alloyed Ti-V and Ti-V-Co solid solutions. The vertical dashed line indicates the change in (110) peak position that occurred after the chemical modification by Co atoms

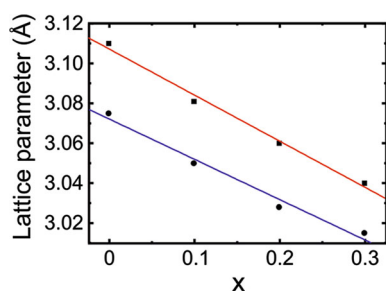


Fig. 2 Lattice parameter vs. Co content in $\text{Ti}_{0.5}\text{V}_{1.5-x}\text{Co}_x$ (filled square) and $\text{Ti}_{0.5}\text{V}_{1.4-x}\text{Ni}_{0.1}\text{Co}_x$ (filled circle)

Table 1 Refined structure parameters of Ti-V-Co alloys

Sample	a , Å	V , Å ³	R_{wp} , %
$\text{Ti}_{0.5}\text{V}_{1.5}$	3.110	30.08	4.3
$\text{Ti}_{0.5}\text{V}_{1.4}\text{Co}_{0.1}$	3.081	29.25	2.5
$\text{Ti}_{0.5}\text{V}_{1.3}\text{Co}_{0.2}$	3.060	28.65	2.2
$\text{Ti}_{0.5}\text{V}_{1.2}\text{Co}_{0.3}$	3.040	28.09	2.0
R_{wp} final weighted average Bragg R -factor			

Table 2 Average particle size, crystallites size and lattice strain of $\text{Ti}_{0.5}\text{V}_{1.5-x}\text{Co}_x$ alloys

Sample	Average particle size, μm	Crystallites size, nm	Lattice strain, %
$\text{Ti}_{0.5}\text{V}_{1.5}$	14.6	5.4	1.1
$\text{Ti}_{0.5}\text{V}_{1.4}\text{Co}_{0.1}$	8.2	9.2	1.1
$\text{Ti}_{0.5}\text{V}_{1.3}\text{Co}_{0.2}$	8.3	10.8	1.6
$\text{Ti}_{0.5}\text{V}_{1.2}\text{Co}_{0.3}$	8.9	33.4	1.8

observed for the lattice strain which increased with Co content in the alloys (Table 2).

SEM micrograph and EDS elements maps obtained for $\text{Ti}_{0.5}\text{V}_{1.2}\text{Co}_{0.3}$ alloy are shown in Fig. 3. Based on presented pictures, it is concluded that all elements are dispersed regularly in the whole volume of the alloy. The same chemical homogeneity was also observed for all alloys (not shown here). Chemical formulas of Ti-V-Co alloys defined based on EDS studies are presented in Table S1 (supplementary data). Despite the fact that these compositions differ from those assumed, the differences are insignificant and should be connected to the accuracy of this measuring technique.

Figure S1 (supplementary data) shows SEM micrographs of obtained $\text{Ti}_{0.5}\text{V}_{1.5-x}\text{Co}_x$ solid solutions. Ti-V-Co alloy particles are porous, cleavage and fracture which are characteristic of MA materials. Their shape is mostly irregular. Moreover, the particles size shows bimodal character—near 1 μm particles are agglomerated into bigger forms (about 50 μm). Figure S2 (supplementary data) shows particle size dimension distribution histograms of $\text{Ti}_{0.5}\text{V}_{1.5-x}\text{Co}_x$ alloys. Table 2 presents the average particle sizes of tested materials. The particles size is decreased after substitution of V by Co atoms. The size is reduced from 14.6 μm to about 8 μm after chemical modification by Co atoms. The reduction of BCC phase particle size caused by Co addition was also observed for inductive melted Ti-V-based materials (Ref 9).

Figure 4 shows the precise morphology of unmodified $\text{Ti}_{0.5}\text{V}_{1.5}$ alloy. Figure 4(a) presents a TEM image of a single grain. Additionally, HRTEM micrograph (Fig. 4b) presents multicrystalline structure—differently oriented nanocrystals are arranged in more complex forms. The $d_{(100)}$ and $d_{(200)}$ spacing values match to refined values from Rietveld method (Fig. 4b).

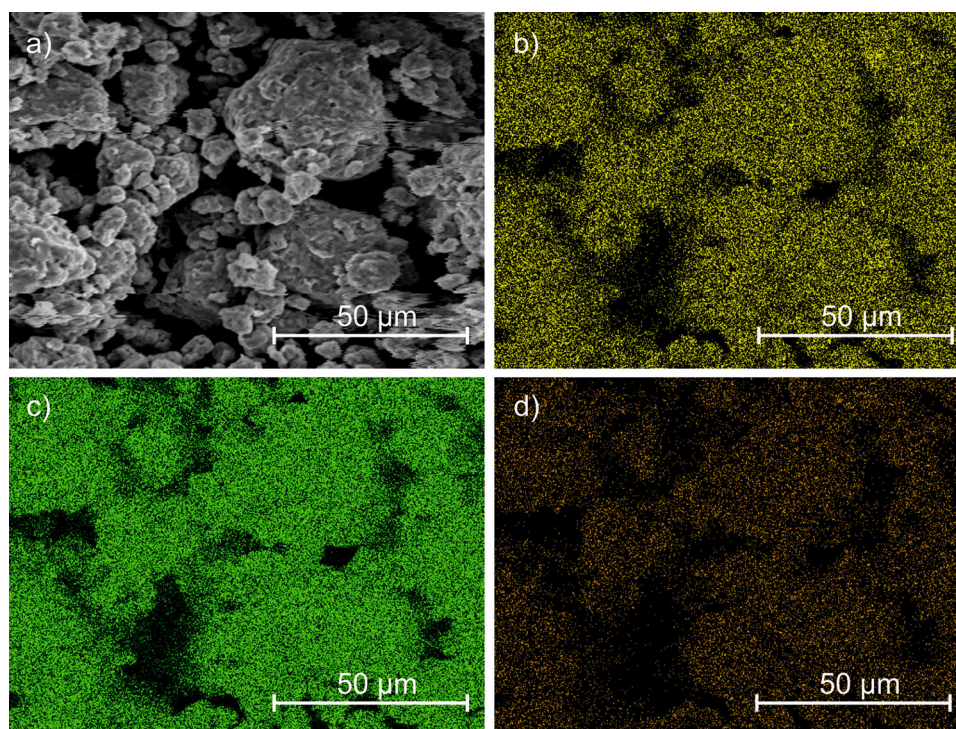


Fig. 3 SEM micrograph of $\text{Ti}_{0.5}\text{V}_{1.2}\text{Co}_{0.3}$ alloy (a) and EDS element maps of Ti $K\alpha_1$ (b), V $K\alpha_1$ (c) and Co $K\alpha_1$ (d)

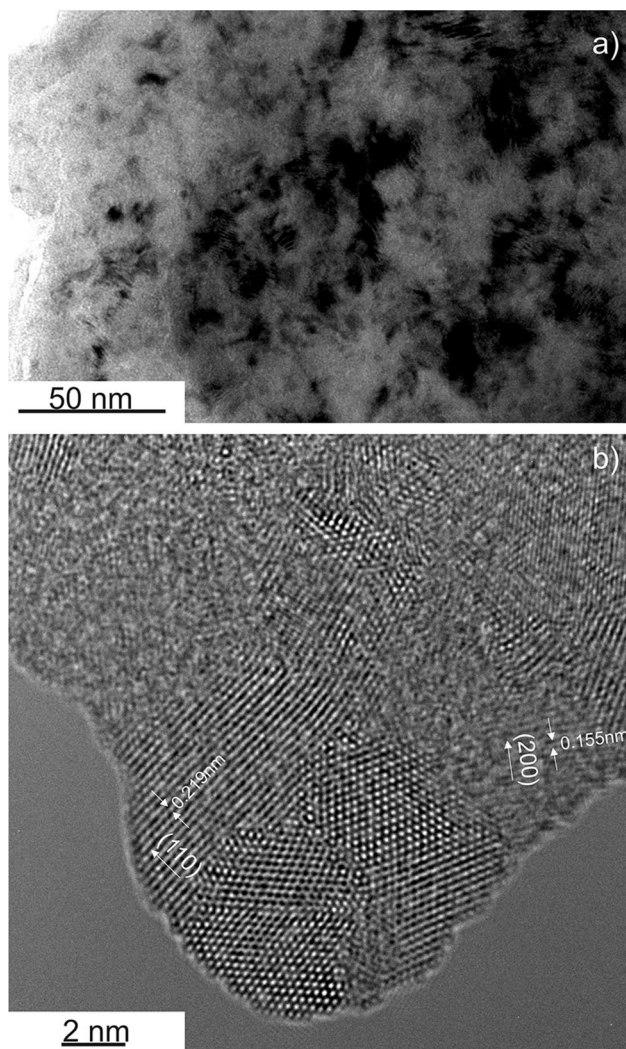


Fig. 4 TEM (a) and HRTEM images (b) of $\text{Ti}_{0.5}\text{V}_{1.5}$ alloy

3.2 Hydrogen Storage Properties

It is noteworthy that there was no activation of alloys before the kinetic measurements. As was shown in the previously published paper, $\text{Ti}_{0.5}\text{V}_{1.5}$ alloy does not absorb hydrogen in the first cycle of test (Ref 4). $\text{Ti}_{0.5}\text{V}_{1.5-x}\text{Co}_x$ alloy powders were also inactive during the initial cycle of tests (not shown here). This should be connected to an oxide layer which covers the particles and restrains from the hydrogenation of materials (Ref 5, 14).

Time-capacity curves of Ti-V and Ti-V-Co solid solutions in second cycle of kinetic measurements are presented in Fig. 5. These curves show that all of studied alloys are in the active state just after the first cycle and followed degassing procedure (under vacuum and at 673 K). The first cycle of kinetic measurement acts as activation in which hydrogen molecules reduce the oxide on the particles surface. These data show that activation of studied BCC alloys is not difficult and the activated alloys actively absorb hydrogen without any incubation time. The absence of incubation time results most likely from nanocrystallinity of studied alloys (shown in Fig. 4). Nanocrystalline materials are characterized by the great number of grain boundaries. Hydrogen can diffuse on the grain

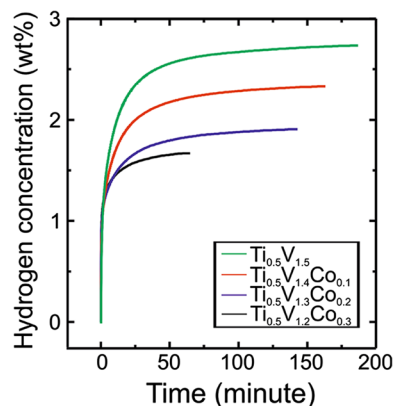


Fig. 5 Second cycles of kinetic measurements performed on $\text{Ti}_{0.5}\text{V}_{1.5-x}\text{Co}_x$ solid solutions

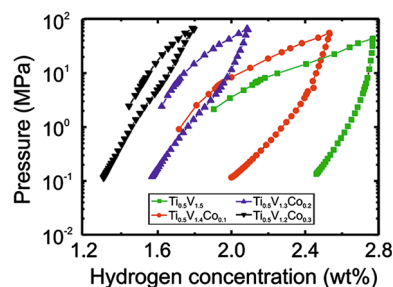


Fig. 6 Pressure-composition isotherms obtained for $\text{Ti}_{0.5}\text{V}_{1.5-x}\text{Co}_x$ solid solutions at 303 K. The upperpart of each curve refers to hydrogen sorption process and the lower part refers to hydrogen desorption process

boundaries more easily than in the bulk region. Therefore, the hydrogen diffusion path is shorter in nanocrystalline materials.

The hydrogen storage capacities depend on the alloy chemical composition. Unmodified $\text{Ti}_{0.5}\text{V}_{1.5}$ alloy can store up to 2.75 wt.%. Increase in Co content caused gradual decrease in the storage capacity which finally reached 1.67 wt.% for $\text{Ti}_{0.5}\text{V}_{1.2}\text{Co}_{0.3}$. It could be caused by the inhomogeneity of materials chemical composition—a part of alloy powder could be composed of elements unreacted during MA process. Therefore, the effective mass of hydrogen-absorbing material could be reduced. However, as was shown in Fig. 3, there are no inhomogeneity in studied materials. The real reason is the Co gives rise to the decrease in the lattice parameter of BCC phase reducing the interstitial sites for hydrogen storage, and thus, the stability of the hydride phase is lowered.

The hydrogenation process kinetics of studied alloys was compared using the time needed to absorbed 95% of maximum hydrogen capacity. This time is highly depended on the alloy elemental composition. It was reduced from more than 1 h for $\text{Ti}_{0.5}\text{V}_{1.5}$ alloy to less than 30 min for Co-rich solid solution.

Figure 6 presents P-C isotherms obtained for $\text{Ti}_{0.5}\text{V}_{1.5-x}\text{Co}_x$ solid solutions at 303 K. These curves are sloped which makes impossible to determine a plateau pressure. Previously published papers indicate that the plateau pressure of V-rich solid solutions is much lower than 0.1 MPa and therefore is not observed on presented in this work curves (Ref 4, 15, 16). It can be seen that the slope increases with higher Co concentration in the alloys. It is also visible that there is a hysteresis

between two parts of each curve (sorption/desorption). The differences between both parts got bigger while the Co content in alloy increased. The same tendency was previously observed for BCC-based alloys chemically modified by Cr (Ref 15). The hydrogen uptakes observed on PC isotherm curves fit to those from the kinetic measurements.

Hydrogen desorption characteristics of measured materials were numerically given by the reversibility of hydriding–dehydriding: 11, 21, 25, 27%, respectively, for $\text{Ti}_{0.5}\text{V}_{1.5}$, $\text{Ti}_{0.5}\text{V}_{1.4}\text{Co}_{0.1}$, $\text{Ti}_{0.5}\text{V}_{1.3}\text{Co}_{0.2}$ and $\text{Ti}_{0.5}\text{V}_{1.2}\text{Co}_{0.3}$ alloys. Ti-V and Ti-V-Co materials showed low reversibility at 303 K. However, the improvement of reversibility was observed in chemically modified alloys. The improvement of reversibility results from changes in the cell volume. The smaller interstitial sites are caused by chemical modification the less stability of hydride phase, and therefore, the reversibility increases. A similar effect of chemical modification on desorption characteristics was shown in the past for different BCC-based alloys (Ref 17). Slight reversibility is connected to low desorption plateau pressures. The plateau region occurs most likely at so low pressure that its measurement exceeds device's capabilities, and therefore, most of hydrogen is not desorbed in the ambient conditions. The reversible capacity can be greatly improved by rising the desorption temperature above 373 K (Ref 5). In order to fully understand the hydrogen storage properties, an electronic study need to be conducted.

$\text{Ti}_{0.5}\text{V}_{1.5-x}\text{Co}_x$ alloys in hydrogenated state were measured by XRD and DSC techniques. X-ray diffractograms of Ti-V and Ti-V-Co solid solutions after hydrogenation are shown on Fig. 7. Almost all patterns (with exception for $\text{Ti}_{0.5}\text{V}_{1.2}\text{Co}_{0.3}$ alloy) consist of peaks which belong to two phases: distorted BCC phase (α -phase) and body-centered tetragonal (BCT) phase (β -phase). The cell volume of distorted BCC α -phase is greater by 3.4–3.7 Å³ after the hydrogen sorption (conclusion from refinement of x-ray data). This volume increase results from the diffusion of H atoms which fill the interstitial sites of BCC solid solution. The fully hydrogenated BCC α -phase stores 1.5 wt.% (Ref 5). The α -phase is characterized by the high stability which prevents the hydrogen desorption at 303 K (Ref 18).

Further sorption of hydrogen caused increase in cell unit along the c axis. Therefore, the structure of alloy changes from distorted BCC hydride to BCT hydride phase (I_4/mmm space group). The lattice parameter a in BCT phase is almost the same

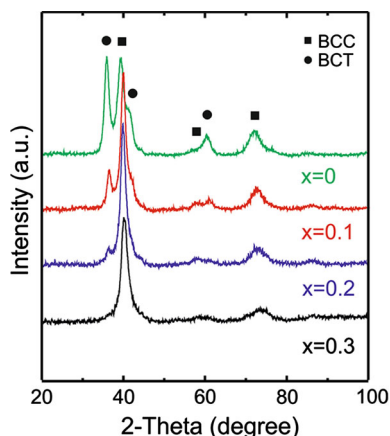


Fig. 7 X-ray diffractograms of fully hydrogenated $\text{Ti}_{0.5}\text{V}_{1.5-x}\text{Co}_x$ solid solutions

for all studied compositions. On the other hand, lattice parameter c increases linearly as a function of the hydrogen concentration (Ref 19). BCT phase is a monohydride structure which can absorb up to 1.9 wt.% (Ref 5). It is easy to see that the increase of Co content in $\text{Ti}_{0.5}\text{V}_{1.5-x}\text{Co}_x$ alloy affects the phase abundance of BCT phase—from 32.3% for $\text{Ti}_{0.5}\text{V}_{1.5}$ to 0% for $\text{Ti}_{0.5}\text{V}_{1.2}\text{Co}_{0.3}$ solid solution. The Rietveld refinement of x-ray patterns obtained for $\text{Ti}_{0.5}\text{V}_{1.5}$ and $\text{Ti}_{0.5}\text{V}_{1.2}\text{Co}_{0.3}$ is presented in Fig. S3 (supplementary data).

The analysis of XRD patterns matches well to the described above result of the hydrogen sorption and desorption studies. The only exception is the analysis of the unmodified Ti-V alloy. The hydrogen uptake measured for this material exceeds 1.9 wt.% which is the maximum hydrogen capacity of BCT phase. As was shown in the previously published paper, the structure of $\text{Ti}_{0.5}\text{V}_{1.5}$ alloy after its fully saturation transforms partially to FCC hydride phase (Ref 4). It is a fully hydrogenated phase that crystallizes in a Fm-3 m space group and can store up to 4 wt.% (Ref 5). This phase is characterized by the highest hydrogen concentration and the lowest stability, and therefore, FCC is the most wanted phase from the application point of view.

DSC profiles obtained for $\text{Ti}_{0.5}\text{V}_{1.5-x}\text{Co}_x$ alloys hydrides are shown on Fig. 8. There are three peaks which are visible on the thermal decomposition curves of hydrogenated $\text{Ti}_{0.5}\text{V}_{1.5}$ solid solution. As was discussed in the previous work, the first one that occurs near to 532 K is most likely connected to transition of FCC to BCT phase. The second peak (peak visible at 631 K) corresponds to the BCT decomposition process. As a result, a distorted BCC hydride phase is obtained. Lastly, the peak visible at 716 K should be connected with the final part of the decomposition process where the dehydrogenated solid solution is obtained (Ref 4). The same hydride decomposition process was described by Kumar et al. for Ti-Cr-C-Co BCC solid solutions (Ref 7).

For $\text{Ti}_{0.5}\text{V}_{1.4}\text{Co}_{0.1}$ alloy, the low temperature hydrogen desorption peak is not visible. It means that FCC hydride phase was not formed. The BCT to BCC hydride phase decomposition temperature was reduced when a part of V in $\text{Ti}_{0.5}\text{V}_{1.5}$ alloy was replaced by Co atoms. It means that the thermal stability of BCT hydride phase was reduced after the chemical modification. Cobalt as late d-block transition metal element has more d-electrons and therefore, basically decrease the hydrogen desorption temperature by decreasing the stability of the hydride phase (Ref 7).

On DSC curves obtained for $\text{Ti}_{0.5}\text{V}_{1.3}\text{Co}_{0.2}$ and $\text{Ti}_{0.5}\text{V}_{1.2}\text{Co}_{0.3}$ alloys visible is only one endothermic peak of final decomposition process. It should be noticed that the higher Co

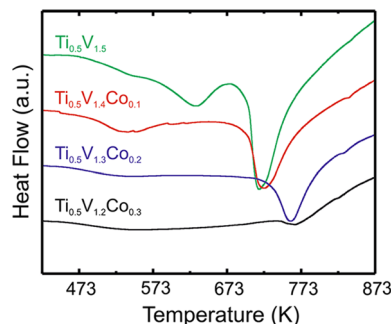


Fig. 8 DSC curves of $\text{Ti}_{0.5}\text{V}_{1.5-x}\text{Co}_x$ alloys hydrides

content caused increase in the decomposition temperature from 716.4 to 765.2 K. The higher the temperature, the higher the stability of hydride phase is. This fits well to the PCI desorption curves and proves the high stability of the hydrogenated BCC phase. Kumar et al. (Ref 20) have shown that the reduction in materials particle size (caused for example by cycled hydrogenation/dehydrogenation process) can decrease the thermal stability of hydride phase. Similar effect of the desorption peak temperature increase was observed in the past for Fe and Cr modified BCC alloys (Ref 15, 21). However, as stated Hang et al. (Ref 15), the main decomposition peak was associated with BCT to BCC hydride decomposition reaction rather than with BCC hydride to dehydrogenated BCC decomposition reaction. The enthalpy of final hydrogen desorption process equals 240.3, 217.7, 108.5 and 10.4 J g⁻¹, respectively, for $x = 0, 0.1, 0.2$ and 0.3 . Therefore, it can be concluded that the chemical modification of V-rich BCC alloys by Co atoms reduces the stability of α phase.

3.3 Discharge Capacity and Cycling Stability

Results of electrochemical studies of $\text{Ti}_{0.5}\text{V}_{1.5-x}\text{Co}_x$ solid solutions are presented in Fig. 9a. All of discharge capacities that are shown in this work are the capacities calculated per unit gram of measured alloy. Unfortunately, $\text{Ti}_{0.5}\text{V}_{1.5}$ alloy is not able to work as a negative electrode material in Ni-MH_x system. Chemical modification of BCC alloy by Co caused slight improvement of the discharge capacity. However, the highest discharge capacity obtained for Ti-V-Co alloys did not exceed 20 mAh g⁻¹, which indicates that these solid solutions are unsuitable for Ni-MH_x negative electrodes. For these reason, these measurements were not fully described.

Due to very poor electrochemical properties of Ti-V-Co alloys, author decided to substitute a part of V by Ni atoms—Ni is often used to catalyse the reaction in Ni-MH_x system (Ref 9). Figure 2 shows the lattice parameter versus Co content in $\text{Ti}_{0.5}\text{V}_{1.4-x}\text{Ni}_{0.1}\text{Co}_x$ solid solutions. The differences between lattice parameters of $\text{Ti}_{0.5}\text{V}_{1.5-x}\text{Co}_x$ and corresponding $\text{Ti}_{0.5}\text{V}_{1.4-x}\text{Ni}_{0.1}\text{Co}_x$ solid solutions are because nickel and vanadium atoms differ in their radius (Ni—0.124 nm; V—0.134 nm).

Figure 9b shows results of electrochemical measurements performed on $\text{Ti}_{0.5}\text{V}_{1.4-x}\text{Ni}_{0.1}\text{Co}_x$ alloys. Table 3 contains the most relevant data from these studies. Chemical modification of

Ti-V-Co alloys by Ni atoms significantly improved the electrochemical properties.

$\text{Ti}_{0.5}\text{V}_{1.4}\text{Ni}_{0.1}$ alloy displayed maximum capacity at 7th cycle. Substitution of V by Co caused improvement of activation properties—all Ti-V-Ni-Co alloys were fully activated after 5 charging/discharging cycles. Maximum discharge capacity was just slightly changed after the chemical modification by Co and reached about 70 mAh/g. With next cycles of charging and discharging, a gradual degradation of discharge capacity was observed. The worsening of electrochemical properties can be caused by a few reasons:

- dissolution of electrode atoms into the KOH solution (Ref 11, 18, 22). As reported Chen et al. addition of Co reduces the dissolution of vanadium and enhances the antioxidation properties (Ref 8, 9).
- creation of an oxide layer (TiO_2) on the particle surface, which is characterized by the very low electrical conductivity and the low hydrogen diffusivity (Ref 22). TiO_2 surface layer stops the dissolution of electrode atoms into the KOH solution (Ref 23).
- pulverization resulted from the volume expansion and the shrinkage which originate from the hydrogen sorption and desorption. As was shown by Miao et al., Co addition can weaken the pulverization process. Moreover, the observed particle size refinement can also increase the pulverization resistance (Ref 9).

It should also be noted that a small portion of alloy particles was found on the bottom of measuring cell after charging/discharging cycles. It suggests that a piece of material brakes away from the rest of electrode during charging/discharging cycles. Reduction in the amount of the electrode material effects in decrease of discharge capacity in next electrode working cycles.

The cyclability of electrodes was improved by chemical modification of BCC alloys. While V atoms dissolve in KOH solution during cyclic charging/discharging, the effective mass of working electrode reduces and therefore the discharge capacity decreases. The dissolution of V atoms in KOH solution is restricted by Co atoms (Ref 8, 9). Moreover, the improvement of cycling stability in Ti-V-Ni-Co alloys can result from noticeable depression of the lattice expansion and pulverization of the alloy particles upon charge/discharge cycling (Ref 9). The only one alloy characterized by worse electrochemical properties was the one with the highest Co content. $\text{Ti}_{0.5}\text{V}_{1.3}\text{Co}_{0.2}$ worked the most stable during electrochemical measurements. The obtained results differ from these obtained in the past for BCC-based alloy for which electrochemical

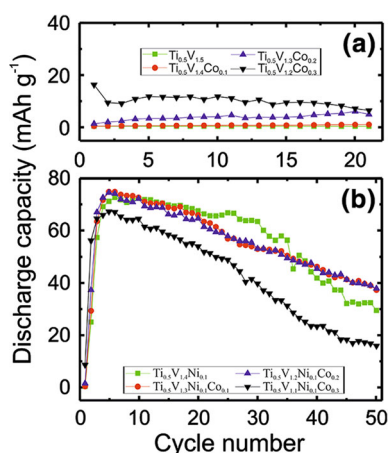


Fig. 9 Results of electrochemical studies performed on: (a) $\text{Ti}_{0.5}\text{V}_{1.5-x}\text{Co}_x$, (b) $\text{Ti}_{0.5}\text{V}_{1.4-x}\text{Ni}_{0.1}\text{Co}_x$ alloys

Table 3 Most relevant data from electrochemical measurements of $\text{Ti}_{0.5}\text{V}_{1.4-x}\text{Ni}_{0.1}\text{Co}_x$ materials

Alloy	Activation cycles	Maximum discharge capacity, mAh/g	R_h , %
$\text{Ti}_{0.5}\text{V}_{1.4}\text{Ni}_{0.1}$	7	72	41
$\text{Ti}_{0.5}\text{V}_{1.3}\text{Ni}_{0.1}\text{Co}_{0.1}$	5	75	47
$\text{Ti}_{0.5}\text{V}_{1.2}\text{Ni}_{0.1}\text{Co}_{0.2}$	5	75	48
$\text{Ti}_{0.5}\text{V}_{1.1}\text{Ni}_{0.1}\text{Co}_{0.3}$	5	67	23
R_h capacity retaining rate after 50th cycle			

properties resulted from properties of C14 Laves secondary phase strongly (Ref 11).

4. Conclusions

$\text{Ti}_{0.5}\text{V}_{1.5-x}\text{Co}_x$ and $\text{Ti}_{0.5}\text{V}_{1.4-x}\text{Ni}_{0.1}\text{Co}_x$ solid solutions ($x = 0, 0.1, 0.2, 0.3$) were synthesized by MA technique. Hydrogenation/dehydrogenation and electrochemical properties of BCC alloys were studied in this work. X-ray diffraction studies have shown all alloys were single-phase BCC solid solution materials. All of the materials were characterized by good homogeneity. HRTEM image has shown creation of differently oriented nanocrystals which were arranged in more complex forms. X-ray diffraction and hydrogenation tests have shown the hydrogenation performance of BCC alloys results from chemical compositions and lattice parameters. BCC alloys are characterized by good activation properties. Moreover, activated alloys can absorb hydrogen without any incubation time. The hydrogen storage capacity reduces with increase in number of Co atoms in the alloy. However, Co improves hydrogenation kinetics, reduces hysteresis and increases reversibility of hydrogen sorption process. Ti-V-Co alloys poorly absorb hydrogen in 6 M KOH solution which is most likely caused by the high stability of hydride phase. Nevertheless, the electrochemical properties can be improved by the chemical modification of BCC alloys by Ni atoms. $\text{Ti}_{0.5}\text{V}_{1.4-x}\text{Ni}_{0.1}\text{Co}_x$ alloys are characterized by better activation properties and improved cyclability in comparison to Co-free $\text{Ti}_{0.5}\text{V}_{1.4}\text{Ni}_{0.1}$ alloy. The chemical modification of BCC alloys by Co atoms is also economically justified due to the 4-5 times higher price of V than Co.

Acknowledgments

Financial assistance from National Science Centre, Poland (no. 2015/17/N/ST8/00271).

References

1. T. Bibienne, M. Tousignant, J.L. Bobet, and J. Hout, Synthesis and Hydrogen Sorption Properties of $\text{TiV}_{(2-x)}\text{Mn}_x$ BCC Alloys, *J. Alloys Compd.*, 2015, **624**, p 247–250. <https://doi.org/10.1016/j.jallcom.2014.11.060>
2. X.B. Yu, Z.X. Yang, S.L. Feng, Z. Wu, and N.X. Xu, Influence of Fe Addition on Hydrogen Storage Characteristics of Ti-V-Based Alloy, *Int. J. Hydrog. Energy*, 2006, **31**, p 1176–1181. <https://doi.org/10.1016/j.ijhydene.2005.09.008>
3. T. Mouri and H. Iba, Hydrogen-Absorbing Alloys with a Large Capacity for a New Energy Carrier, *Mater. Sci. Eng., A*, 2002, **329–331**, p 346–350. [https://doi.org/10.1016/S0921-5093\(01\)01597-0](https://doi.org/10.1016/S0921-5093(01)01597-0)
4. M. Balcerzak, Structure and Hydrogen Storage Properties of Mechanically Alloyed Ti-V alloys, *Int. J. Hydrog. Energy*, 2017, **42**, p 23698–23707. <https://doi.org/10.1016/j.ijhydene.2017.03.224>
5. S. Challet, M. Latroche, and F. Heurtaux, Processing and Microstructural Characterization of a Ti-Cr-Nb Alloy Synthesized by High-Energy Ball-Milling, *J. Alloys Compd.*, 2007, **439**, p 294–301. <https://doi.org/10.1016/j.jallcom.2006.08.070>
6. T. Tamura, T. Kuriwa, T. Amemiya, T. Fuda, A. Kamegawa, H. Takamura, and M. Okada, New Vanadium-Based Protium Absorbing Alloys with Laves Phases Along Grain Boundary, *Mater. Trans.*, 1999, **40**, p 431–434
7. A. Kumar, S. Banerjee, C.G.S. Pillai, and S.R. Bharadwaj, Hydrogen Storage Properties of $\text{Ti}_{2-x}\text{CrV}_x$ ($\text{M}=\text{Fe}, \text{Co}, \text{Ni}$) Alloys, *Int. J. Hydrog. Energy*, 2013, **38**, p 13335–13342. <https://doi.org/10.1016/j.ijhydene.2013.07.096>
8. L.X. Chen, R. Guo, Y.Q. Lei, F.B. Dai, L. Li, B. Liao, C.P. Chen, and Q.D. Wang, Phase Structures and Electrochemical Performance of $\text{V}_{2.1}\text{TiNi}_{0.5}\text{Hf}_{0.05}\text{Co}_x$ ($x = 0-0.192$) Hydrogen Storage Alloys, *J. Alloys Compd.*, 2005, **404–406**, p 657–660. <https://doi.org/10.1016/j.jallcom.2004.09.085>
9. H. Miao, M. Gao, Y. Liu, D. Zhu, and H. Pan, An Improvement on Cycling Stability of Ti-V-Fe-Based Hydrogen Storage Alloys with Co Substitution for Ni, *J. Power Sources*, 2008, **184**, p 627–632. <https://doi.org/10.1016/j.jpowsour.2008.02.065>
10. M. Balcerzak, Effect of Ni on Electrochemical and hydrogen Storage Properties of V-Rich Body-Centered-Cubic Solid Solution Alloys, *Int. J. Hydrog. Energy*, 2018, **43**, p 8395–8403. <https://doi.org/10.1016/j.ijhydene.2018.03.123>
11. Q.A. Zhang, Y.Q. Lei, X.G. Yang, Y.L. Du, and Q.D. Wang, Phase Structures and Electrochemical Properties of $\text{V}_3\text{TiNi}_{0.56}\text{Hf}_{0.24}\text{Co}_x$ Alloys, *J. Alloys Compd.*, 2000, **296**, p 87–91. [https://doi.org/10.1016/S0925-8388\(99\)00520-4](https://doi.org/10.1016/S0925-8388(99)00520-4)
12. K. Young, T. Ouchi, J. Nei, and T. Meng, Effects of Cr, Zr, V, Mn, Fe, and Co to the Hydride Properties of Laves Phase-Related Body-Centered-Cubic Solid Solution Alloys, *J. Power Sources*, 2015, **281**, p 164–172. <https://doi.org/10.1016/j.jpowsour.2015.01.170>
13. M. Balcerzak, M. Nowak, and M. Jurczyk, Hydrogenation and Electrochemical Studies of La-Mg-Ni Alloys, *Int. J. Hydrog. Energy*, 2017, **42**, p 1436–1443. <https://doi.org/10.1016/j.ijhydene.2017.03.224>
14. Z. Hang, X. Xiao, D. Tan, Z. He, W. Li, S. Li, C. Chen, and L. Chen, Microstructure and Hydrogen Storage Properties of $\text{Ti}_{10}\text{V}_{84-x}\text{Fe}_x\text{Zr}_x$ ($x = 1-8$) Alloys, *Int. J. Hydrog. Energy*, 2010, **35**, p 3080–3086. <https://doi.org/10.1016/j.ijhydene.2009.07.019>
15. Z. Hang, L. Chen, X. Hiao, S. Li, C. Chen, Y. Lei, and Q. Wang, The Effect of Cr Content on the Structural and Hydrogen Storage Characteristics of $\text{Ti}_{10}\text{V}_{80-x}\text{Fe}_x\text{Zr}_x$ ($x = 0-14$) Alloys, *J. Alloys Compd.*, 2010, **493**, p 396–400. <https://doi.org/10.1016/j.jallcom.2009.12.110>
16. K. Nomura and E. Akiba, H_2 Absorbing–Desorbing Characterization of the Ti-V-Fe Alloy System, *J. Alloys Compd.*, 1995, **231**, p 513–517. [https://doi.org/10.1016/0925-8388\(95\)01862-X](https://doi.org/10.1016/0925-8388(95)01862-X)
17. M.V. Lototsky, V.A. Yartys, and I.Y. Zavaliy, Vanadium-Based BCC Alloys: Phase-Structural Characteristics and Hydrogen Sorption Properties, *J. Alloys Compd.*, 2005, **404**, p 421–426. <https://doi.org/10.1016/j.jallcom.2005.01.139>
18. M. Tsukahara, K. Takahashi, T. Mishima, T. Sakai, H. Miyamura, N. Kuriyama, and I. Uehara, Metal Hydride Electrodes Based on Solid Solution Type Alloy TiV_3Ni_x ($0 \leq x \leq 0.75$), *J. Alloys Compd.*, 1995, **226**, p 203–207. [https://doi.org/10.1016/0925-8388\(95\)01570-1](https://doi.org/10.1016/0925-8388(95)01570-1)
19. B. Massicot, M. Latroche, and J.M. Joubert, Hydrogenation Properties of Fe-Ti-V BCC Alloys, *J. Alloys Compd.*, 2011, **509**, p 372–379. <https://doi.org/10.1016/j.jallcom.2010.09.030>
20. A. Kumar, K. Shashikala, S. Banerjee, J. Nuwad, P. Das, and C.G.S. Pillai, Effect of Cycling on Hydrogen Storage Properties of Ti_2CrV Alloy, *Int. J. Hydrog. Energy*, 2012, **37**, p 3677–3682. <https://doi.org/10.1016/j.ijhydene.2011.04.135>
21. Z. Hang, X. Xiao, K. Yu, S. Li, C. Chen, and L. Chen, Influence of Fe Content on the Microstructure and Hydrogen Storage Properties of $\text{Ti}_{16}\text{Zr}_5\text{Cr}_{22}\text{V}_{57-x}\text{Fe}_x$ ($x = 2-8$) Alloys, *Int. J. Hydrog. Energy*, 2010, **35**, p 8143–8148. <https://doi.org/10.1016/j.ijhydene.2009.12.184>
22. J.H. Kim, H. Lee, P.S. Lee, C.Y. Seo, and J.Y. Lee, A Study on the Improvement of the Cyclic Durability by Cr Substitution in V-Ti Alloy and Surface Modification by the Ball-Milling Process, *J. Alloys Compd.*, 2003, **348**, p 293–300. [https://doi.org/10.1016/S0925-8388\(02\)00801-0](https://doi.org/10.1016/S0925-8388(02)00801-0)
23. C. Iwakura, R. Shin-ya, K. Miyanohara, S. Nohara, and H. Inoue, Effects of Ti-V Substitution on Electrochemical and Structural Characteristics of MgNi Alloy Prepared by Mechanical Alloying, *Electrochim. Acta*, 2001, **46**, p 2781–2786. [https://doi.org/10.1016/S0134-6866\(01\)00513-8](https://doi.org/10.1016/S0134-6866(01)00513-8)

Publisher's Note Springer Nature remains neutral with regard to jurisdictional claims in published maps and institutional affiliations.